

A multiscale and multicriteria Generative Adversarial Network to synthesize 1-dimensional turbulent fields

Carlos Granero Belinchon^{1,2} & Manuel Cabeza Gallucci^{1,3}

¹ Department of Mathematical and Electrical Engineering, IMT Atlantique, Lab-STICC, UMR CNRS 6285, 655 Av. du Technopôle, Plouzané, 29280, Bretagne, France.

² Odyssey, Inria/IMT Atlantique, 263 Av. Général Leclerc, Rennes, 35042, Bretagne, France.

³ Electronic Engineering Department, Facultad de Ingeniería, Universidad de Buenos Aires, Paseo Colón 850, C1063ACV, Buenos Aires, Argentina

E-mail: carlos.granero-belinchon@imt-atlantique.fr ; mcabezag@fi.uba.ar

August 2023

Abstract. This article introduces a new Neural Network stochastic model to generate a 1-dimensional stochastic field with turbulent velocity statistics. Both the model architecture and training procedure ground on the Kolmogorov and Obukhov statistical theories of fully developed turbulence, so guaranteeing descriptions of 1) energy distribution, 2) energy cascade and 3) intermittency across scales in agreement with experimental observations. The model is a Generative Adversarial Network with multiple multiscale optimization criteria. First, we use three physics-based criteria: the variance, skewness and flatness of the increments of the generated field that retrieve respectively the turbulent energy distribution, energy cascade and intermittency across scales. Second, the Generative Adversarial Network criterion, based on reproducing statistical distributions, is used on segments of different length of the generated field. Furthermore, to mimic multiscale decompositions frequently used in turbulence's studies, the model architecture is fully convolutional with kernel sizes varying along the multiple layers of the model. To train our model we use turbulent velocity signals from grid turbulence at Modane wind tunnel.

Keywords: TURBULENCE, STOCHASTIC FIELDS, NEURAL NETWORK , GAN

1. Introduction

Turbulent fluids exhibit complex non-linear and multiscale dynamics which can not be described from a deterministic point of view and which lead to a complex statistical behavior of the velocity field of the flow [1, 2, 3, 4]. Therefore, not only second-order but also higher-order statistics are needed to describe turbulent velocity

fields [4]. The generation of stochastic fields with turbulent statistics have been broadly studied [5, 6, 7, 8, 9, 10, 11] and still remain a subject of study [12, 13, 14].

In the last decade, Neural Network (NN) stochastic generative models appeared and gained popularity, from Generative Adversarial Networks (GANs) [15, 16], to generative diffusion models [17, 18, 19] or autoencoders [20, 21]. These models are being currently developed to generate stochastic fields with complex statistical structures [16] and more particularly with turbulent statistical behaviors [22, 23]. Thus, NN stochastic generative models have been used to reproduce turbulent fields for different applications [24, 25, 26, 27]. In order to generate satisfactory stochastic fields these NN approaches need the most of the time to incorporate some physics of turbulence [28, 29, 30, 31, 32]. However, very few of these works incorporate higher-order statistics in the training procedure [29] and the most only evaluate the performances of the NN model to reproduce second-order statistics of the field, mainly the power spectrum or the correlation function [25, 30, 31, 26]. Then, by not evaluating higher-order statistics of the generated field, these works do not study the capacity of their models to reproduce the energy cascade of turbulence [1] or the intermittency phenomenon [2, 3].

In this article we propose a multiscale and multicriteria GAN to generate a 1-dimensional stochastic field with turbulent statistics. This model grounds on the Kolmogorov and Obukhov theories of turbulence [1, 2, 3] and so, contrary to most of the state of the art, it includes second-order and higher-order statistics in both training and evaluation. Consequently, the proposed model is based on the physics of turbulence, and the generated stochastic field correctly reproduces the energy distribution, energy cascade and intermittency of turbulent velocity flows.

Section 2 presents the Kolmogorov-Obukhov theories of fully developed turbulence and the experimental velocity dataset used for training. Section 3 introduces the multiscale and multicriteria physics based GAN approach used to generate a 1d stochastic field with turbulent statistics. Section 4 shows a second and higher-order statistical description of the generated field and the experimental velocity dataset and compares both statistical behaviors. Finally, section 5 presents the main conclusions and perspectives.

2. Fully developed turbulence

2.1. The Kolmogorov-Obukhov theories: energy cascade and intermittency

Fully developed turbulence corresponds to flows at very high Reynolds number, when the nonlinear advection term of the Navier-Stokes equations dominates the dynamics of the flow [4]. In this limit and away from boundaries, the flow is considered statistically isotropic and homogeneous and the Kolmogorov-Obukhov theories provide a statistical description of fully developed turbulence [1, 2, 3].

The Kolmogorov 1941 theory prescribes the existence of three ranges of scales with

different statistical behaviors: the integral domain contains the large scales of the flow where energy is injected, the dissipative domain contains the small scales where energy is dissipated, and the inertial domain contains the scales in between, where the energy cascades from large scales down to smaller ones [4, 1, 33]. Thus, two scales appear naturally, the integral scale L which divides the integral and inertial domains and the Kolmogorov scale η which separates the inertial and dissipative ones.

Following Kolmogorov 1941, we focus on the longitudinal velocity $v(x)$ [1, 4], and we use the increment to define the scale l of turbulent velocity:

$$\delta_l v(x) = v(x + l) - v(x) \quad (1)$$

In the inertial domain of scales $L > l > \eta$, the Kolmogorov 1941 theory states that the structure function of order p , defined as the statistical moment of order p of the velocity increments, behaves as a power law of the scale with exponent $p/3$:

$$S_p(l) = \langle (\delta_l v(x))^p \rangle \propto l^{p/3} \quad (2)$$

where $S_p(l)$ is the structure function of order p and $\langle \rangle$ is the spatial average.

The variance of the velocity increments $S_2(l)$ describes the energy distribution of the flow across scales, and from (2) it behaves as $l^{2/3}$ in the inertial domain. Moreover the 4/5 law of Kolmogorov, directly obtained from the Navier-Stokes equation through the Karman-Howarth development [34], shows the existence of an energy flux in the inertial domain from large to small scales which is related to the third order statistical moment of the velocity increments $S_3(l) \propto -l$. This 4/5 law of Kolmogorov directly relates the energy cascade across scales to the non-Gaussianity of the velocity field.

Finally, Kolmogorov and Obukhov provided a correction to the above theory in 1962 [2, 3]: the energy dissipation in a turbulent flow is non homogeneous and should be considered locally. This leads to a deformation of the probability density function (PDF) of the velocity increments across the scales, from almost Gaussian at large scale to non-Gaussian at small scales. More precisely extreme events of the velocity increments are the more and more intense and the more and more recurrent at small scales. This is known as intermittency, and leads to the following correction to the Kolmogorov 1941 theory:

$$S_p(l) = \langle (\delta_l v(x))^p \rangle \propto l^{\zeta_p} \quad (3)$$

where ζ_p is the scaling exponent which is a non-linear function of p , and from the 4/5 law of Kolmogorov $\zeta_3 = 1$. The non-linear scaling exponent can be measured by fitting the slope of $\log(S_p(l))$ in function of $\log(l)$ in the inertial domain of scales for different orders p .

In order to highlight the non-Gaussian and intermittent nature of turbulence we focus on the skewness and flatness of the velocity increments [35, 4] defined as:

$$\mathcal{S}(l) = \frac{S_3(l)}{S_2(l)^{3/2}} = \frac{\langle (\delta_l v(x))^3 \rangle}{\langle (\delta_l v(x))^2 \rangle^{3/2}} \quad (4)$$

$$\mathcal{F}(l) = \frac{S_4(l)}{S_2(l)^2} = \frac{\langle (\delta_l v(x))^4 \rangle}{(\langle \delta_l v(x) \rangle^2)^2} \quad (5)$$

On the one hand, the skewness characterizes the asymmetry of the PDF of the velocity increments across scales. Symmetric PDFs exhibit zero skewness ($\mathcal{S} = 0$), and from the Kolmogorov 4/5 law, negative values of the skewness in the inertial and dissipative domains reflect the existence of an energy cascade. On the other hand, the flatness characterizes the importance of the tails of the PDF of the velocity increments across scales. A Gaussian PDF is characterized by $\mathcal{F} = 3$, and so, the flatness of the velocity increments is 3 in the integral domain of scales and increases to non-Gaussian values when the scale decreases. This illustrates the higher importance of extreme events in the PDF of the velocity increments at small scales, *i.e.* the intermittent nature of turbulence.

2.2. Modane turbulent velocity dataset

The Modane turbulent velocity dataset consists on Eulerian longitudinal velocity measurements from a grid turbulence setup in the wind tunnel of ONERA at Modane [36]. The mean velocity of the flow is $\langle v \rangle = 20.5 \text{ m/s}$. The measurements are obtained at a sampling frequency of $f_s = 25 \text{ kHz}$ at a fixed point far away from boundaries. The Taylor-scale Reynolds number of the flow is $R_\lambda = 2500$. Then, we consider the flow in fully developed turbulent regime as well as homogeneous and isotropic. We assume Taylor frozen turbulence hypothesis and consider temporal variations as spatial ones [4]. Then, the sampling distance can be expressed as $l_s = \langle v \rangle f_s$. From previous studies, the integral and Kolmogorov scales of the flow are $L = 2350 l_s$ and $\eta = 5 l_s$ [37]. A detailed multiscale statistical characterization of the Modane turbulent velocity dataset is provided in section 4 and in the literature [35, 36, 11, 38].

3. Multiscale and Multicriteria Physics Based GAN

Our Neural Network model is conceived to synthesize a stochastic field $u(x)$ reproducing four main results of the Kolmogorov-Obukhov theory of fully developed turbulence:

- In a turbulent flow we can discriminate **three domains of scales**: integral, inertial and dissipative, each one with a different statistical behavior.
- The **distribution of energy** across scales is described by $S_2(l)$, and in the inertial domain it behaves as $\sim l^{2/3}$.
- The **cascade of energy** is related to the non-Gaussianity of the velocity field through the 4/5 law of Kolmogorov. This implies negative values of the skewness in both the inertial and dissipative domains, as well as $\zeta_3 = 1$.
- **Intermittency** introduces extreme events in the velocity increments at scales in the inertial and dissipative domains. The importance of these extreme events

is characterized by the flatness which tends to Gaussian values at large scales. Intermittency also leads to a non-linear scaling exponent function ζ_p .

Our model is based on the GAN approach first proposed by Goodfellow et al. [15]. However, several modifications have been done to introduce the physics of turbulence into the model. First, the generator model \mathcal{G} follows a fully-convolutional U-Net structure which, similarly to the Kolmogorov-Obukhov theory of turbulence, is based on multiresolution analysis. Second, several multiscale criteria are used during training, each one with an assigned discriminator network. Thus, in order to recover respectively the energy distribution, energy cascade and intermittency of turbulence, three discriminators, \mathcal{D}_{S_2} , $\mathcal{D}_{\mathcal{S}}$ and $\mathcal{D}_{\mathcal{F}}$, compare the $\log(S_2(l))$, $\mathcal{S}(l)$ and $\log(\mathcal{F}/3)$ of the generated field and Modane. These three criteria are also helpful for recovering the three domains of scales of turbulence. Finally a discriminator, $\mathcal{D}_{\text{scale-invariance}}$, compares segments of different sizes of the generated field $u(x)$ and Modane $v(x)$. This criterion searches for exploiting the potentialities of GAN to reproduce the PDFs of Modane data at several scales. It is devoted to reproduce the scale-invariance of turbulence and to impose different statistical dynamics on $u(x)$ at different scales. Figure 1 illustrates this multiscale and multicriteria physics based Generative Adversarial Network approach.

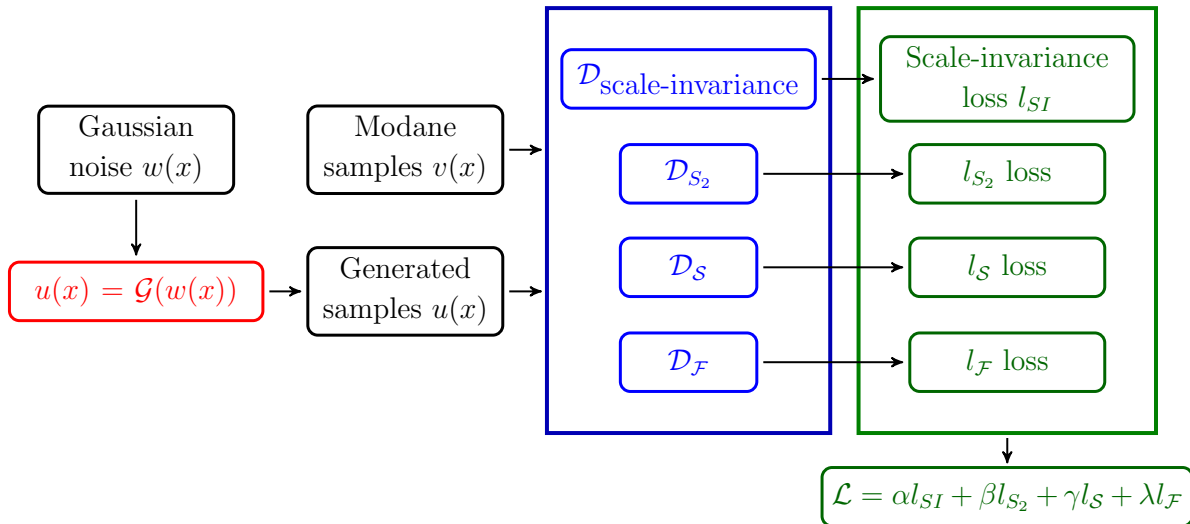


Figure 1. Multiscale and multicriteria physics based GAN. In red the fully convolutional generator model \mathcal{G} which produces realizations of a 1d stochastic field $u(x)$ from realizations of a Gaussian noise $w(x)$. In blue the physics-based discriminators used to train the model. The $\mathcal{D}_{\text{scale-invariance}}$ discriminator is feeded up with Modane realizations $v(x)$ and generated ones $u(x)$, while the other three discriminators are directly feeded up with the corresponding statistics across scales of $v(x)$ and $u(x)$. Each discriminator has its own loss function in green. The total loss function of the GAN, also in green, is a linear combination of the four loss functions of the discriminators.

3.1. The generator model

The generator model \mathcal{G} is fully-convolutional and stochastic:

$$u(x) = \mathcal{G}(w(x)) \quad (6)$$

This model takes as input a 1-dimensional Gaussian white noise $w(x)$ of size N and produces a 1-dimensional field of the same size $u(x)$ with turbulent velocity statistics. Consequently, the model \mathcal{G} operates doubly on the input Gaussian white noise. On the one hand, it deforms the Gaussian PDF of the noise to a PDF in agreement with turbulent velocity statistics, *i.e.* slightly skewed. On the other hand, it introduces a structure of dependencies in the generated field leading to the desired statistical moments of the increments of the field.

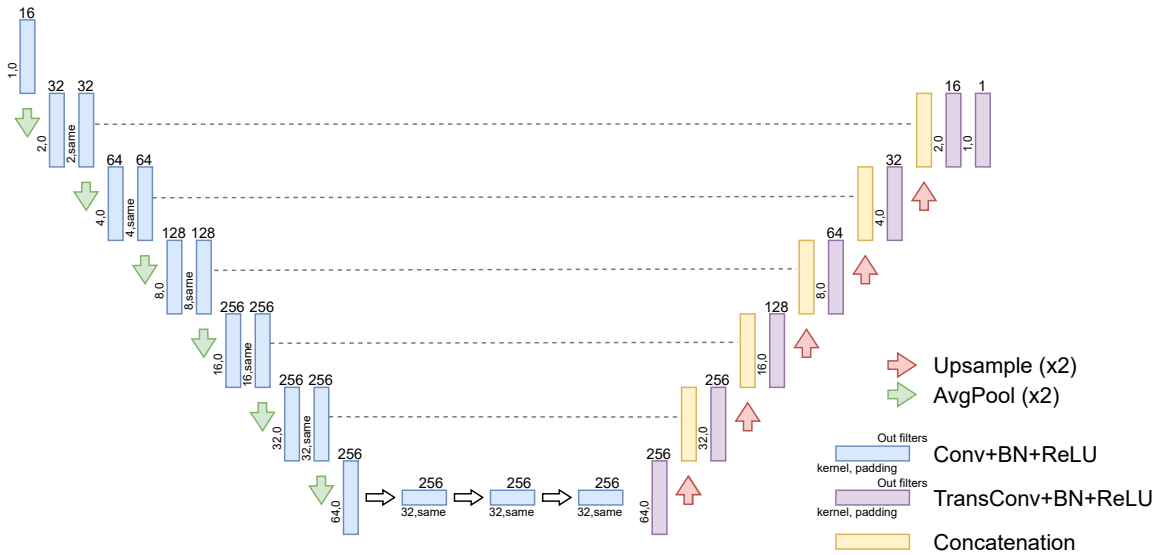


Figure 2. U-Net architecture of \mathcal{G} taking as input a Gaussian white noise $w(x)$ of size N and providing as output a stochastic field with turbulent statistics $u(x)$ of the same size. Convolutional and transpose convolutional blocks made up of a convolutional layer (respectively transpose convolutional layer), batch normalization and ReLU activation function are represented by the blue and purple rectangles respectively. The number at the top of each rectangle indicates the number of channels of the output of the block. The numbers at the left of each rectangle indicate the kernel size of the filter. The used padding is indicated with *same* when the size of the input and output are equal and 0 when there is no padding. The stride used on each convolution and transpose convolution is always 1. Green and red arrows mean respectively average pooling and upsampling. The concatenated long-skip connections are represented by the yellow rectangles.

The model \mathcal{G} follows a U-Net architecture [39] which consists of an encoder followed by its symmetrical decoder both connected by a bridge at the deepest level, see figure 2. On the one hand, our encoder has six levels each one with two convolutional blocks and an average pooling layer. Each convolutional block is defined by a convolutional layer,

batch normalization and ReLU activation function. On the other hand, the decoder has six analogous levels each one defined by a transpose convolutional block (transpose convolution, batch normalization and ReLU activation) and an upsampling layer. The kernel sizes of the convolutions and transpose convolutions increase with the depth of the level and vary from 2 to 64 samples. This together with the pooling allows the model to reproduce the long range dependencies of the turbulent velocity field. The deepest level of the encoder and the decoder are bridged by three convolutional blocks all with a kernel size of 32 samples. Moreover, concatenated long-skip connections link each level of the encoder with the symmetrical level of the decoder. This connections help in keeping the stability of the network during training and minimizing the vanishing gradient effects [40]. Concatenated long-skip connections were used since they provided the best performances in our case study. The generator model has 26 millions of parameters.

3.2. The multiscale and multicriteria discriminators

Three discriminators, \mathcal{D}_{S_2} , \mathcal{D}_S and $\mathcal{D}_{\mathcal{F}}$, are used respectively on the second order structure function $\log(S_2(l))$, the skewness $S(l)$ and the flatness $\log(\mathcal{F}/3)$ of the generated field and Modane. Each one of them uses the GAN's loss derived from the binary cross-entropy [15]. We note the loss functions of these discriminators l_{S_2} , l_S and $l_{\mathcal{F}}$. To define \mathcal{D}_{S_2} , \mathcal{D}_S and $\mathcal{D}_{\mathcal{F}}$, we use dense Neural Networks with 5 hidden layers and 25.000 parameters in total, see figure 3.

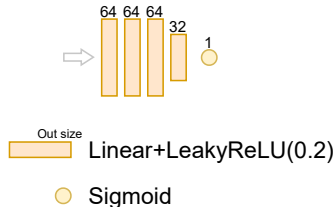


Figure 3. Architecture of the discriminator models \mathcal{D}_{S_2} , \mathcal{D}_S and $\mathcal{D}_{\mathcal{F}}$ which take as input respectively the S_2 , S and \mathcal{F} curves and provide a scalar value in $(0, 1)$. Each yellow rectangle represents a dense layer followed by Leaky ReLU activation, with the number at the top of the rectangle meaning the output size of the dense layer. All Leaky ReLU use a slope of 0.2 for negative values. The yellow circle represents the sigmoid activation function.

The proposed *scale-invariance* discriminator \mathcal{D}_{SI} is made up of four independent convolutional neural networks, each one working on portions of different length of the 1-dimensional fields, see figure 4. So, each NN focuses on information at different scales. Indeed, each NN works respectively on segments of length $N/2$, $N/4$, $N/8$ and $N/16$ derived from the original input of size N , and without overlapping between the segments of same size. Using smaller segments was found to not improve performance, likely due to the non-stationarity of the fields at smaller scales in our case study. The \mathcal{D}_{SI} contains 197.000 parameters altogether.

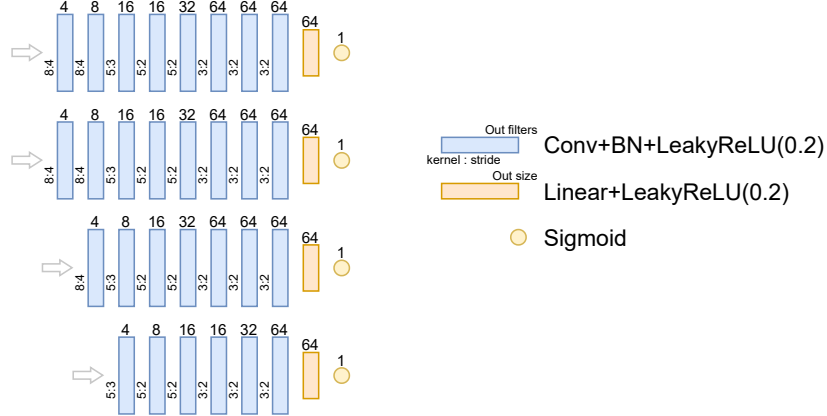


Figure 4. Architecture of the four neural networks defining \mathcal{D}_{SI} . From top to bottom, each row of the discriminator takes as input a signal of size $N/2$, $N/4$, $N/8$ and $N/16$ respectively and provides a scalar value in $(0, 1)$. Blue rectangles represent convolutional blocks made up of a convolutional layer, batch normalization and Leaky ReLU activation function. Yellow rectangles represent dense blocks made up of a dense layer followed by a Leaky Relu activation. The Leaky ReLU activations use a slope 0.2 for negative values. The output size of each linear block is indicated by the number at the top of each rectangle. For convolutional blocks, the kernel size and stride are indicated by the numbers at the left of the blue rectangles and there is no padding. The yellow circle represents the sigmoid activation function.

The loss of \mathcal{D}_{SI} is a weighted sum of the losses of the four convolutional networks:

$$l_{SI} = \sum_{i=1}^2 l_{N/2}^{(i)} + 0.5 \sum_{i=1}^4 l_{N/4}^{(i)} + 0.25 \sum_{i=1}^8 l_{N/8}^{(i)} + 0.125 \sum_{i=1}^{16} l_{N/16}^{(i)} \quad (7)$$

where $l_K^{(i)}$ is the loss of the discriminator network applied on the i th segment of length K and the weights in the linear combination are added to compensate for the increasing number of segments when K decreases. Each one of these losses is calculated using the GAN's loss derived from the binary cross entropy [15].

3.3. Optimization setup

For training the generator and discriminators, we follow the approach proposed in [15] and consider for each discriminator its own loss function and for the generator the loss function defined as:

$$\mathcal{L} = \alpha l_{SI} + \beta l_{S_2} + \gamma l_{\mathcal{S}} + \lambda l_{\mathcal{F}} \quad (8)$$

with hyperparameters α , β , γ and λ . These hyper-parameters were optimized using a grid search with a step of 0.05 and three constraints: the hyper-parameters must sum up to 1, α must be higher than β , γ and λ , and β must be higher than γ and λ . The second constraint was done to maximize the influence of the *scale-invariance* discriminator over the other ones. The third constraint was added since \mathcal{S} and \mathcal{F} depend explicitly on S_2 .

and so, an appropriate second order structure function is needed to correctly model the skewness and flatness. The final parameters $(\alpha, \beta, \gamma, \lambda) = (0.5, 0.2, 0.15, 0.15)$ were found to be optimal under the given constraints.

The model was trained for 500 epochs using a batch size of 32 and signals of length $N = 2^{15}$. The discriminator was trained twice for each generator epoch as in [15]. A learning rate of 0.001 was used for both the generator and discriminators.

4. Results and Discussion

In this section, we statistically characterize the stochastic field $u(x)$ provided by our model. To do so, we generate 256 individual realizations of size $N = 2^{15}$ samples. In order to avoid border effects due to the convolutional nature of our model, the noises $w(x)$ used as inputs of \mathcal{G} are of size $N + N_b$, and we only keep for analysis the N samples in the middle of the output field $u(x)$. N_b is the number of samples impacted by border effects and in our study case $N_b = 8192$. We also characterize the Modane turbulent velocity field $v(x)$ for comparison. With this purpose we use 256 realizations of size N of the Modane turbulent dataset.

Figures 5 a), b) and c) show three realizations of $u(x)$ and d), e) and f) three realizations of $v(x)$. Visually it is very difficult to distinguish the $u(x)$ and $v(x)$ fields. The only small difference comes from the slightly more intense fluctuations of Modane field at very small scale. Besides, we study the variance, skewness and flatness of the increments of the stochastic field $u(x)$ and Modane $v(x)$ across scales. We look also at the PDF of several velocity increments of $u(x)$ and $v(x)$ for scales in the integral, inertial and dissipative domains. Finally, we analyse their scaling function and compare them to the linear behavior described by the Kolmogorov 1941 theory.

Figure 6 shows a) the logarithm of the second order structure function $\log(S_2(l))$, b) the skewness $\mathcal{S}(l)$ and c) the logarithm of the flatness $\log(\mathcal{F}(l)/3)$ in function of the logarithm of the scale of analysis $\log(l/L)$. Curves represent the mean value and errorbars the standard deviation both calculated on 256 realizations. Blue corresponds to the Modane velocity and black to the generated field. Both the black and blue curves of $\log(S_2(l))$ are maximum at large scale $l > L$ where they present a plateau. For scales in the inertial domain $\eta < l < L$ both curves exhibit a linear behavior of slope $\sim 2/3$, while in the dissipative domain $l < \eta$ their slope is steeper and present a value ~ 2 . The skewness of Modane and the generated field are close to zero at large scales $l > L$ and decrease to negative values in the inertial and dissipative domains with a steeper decrease in the dissipative domain. Finally, both curves of flatness are close to zero at large scales, illustrating the Gaussian nature of the fields in the integral domain. In the inertial domain they increase when the scale decreases with $\log(\mathcal{F}(l)/3)$ behaving linearly with a slope -0.1 and this increase is steeper when entering in the dissipative domain.

So, for both the Modane turbulent velocity $v(x)$ and the generated stochastic field $u(x)$, three domains of scales with different statistical behaviors are observed. For both

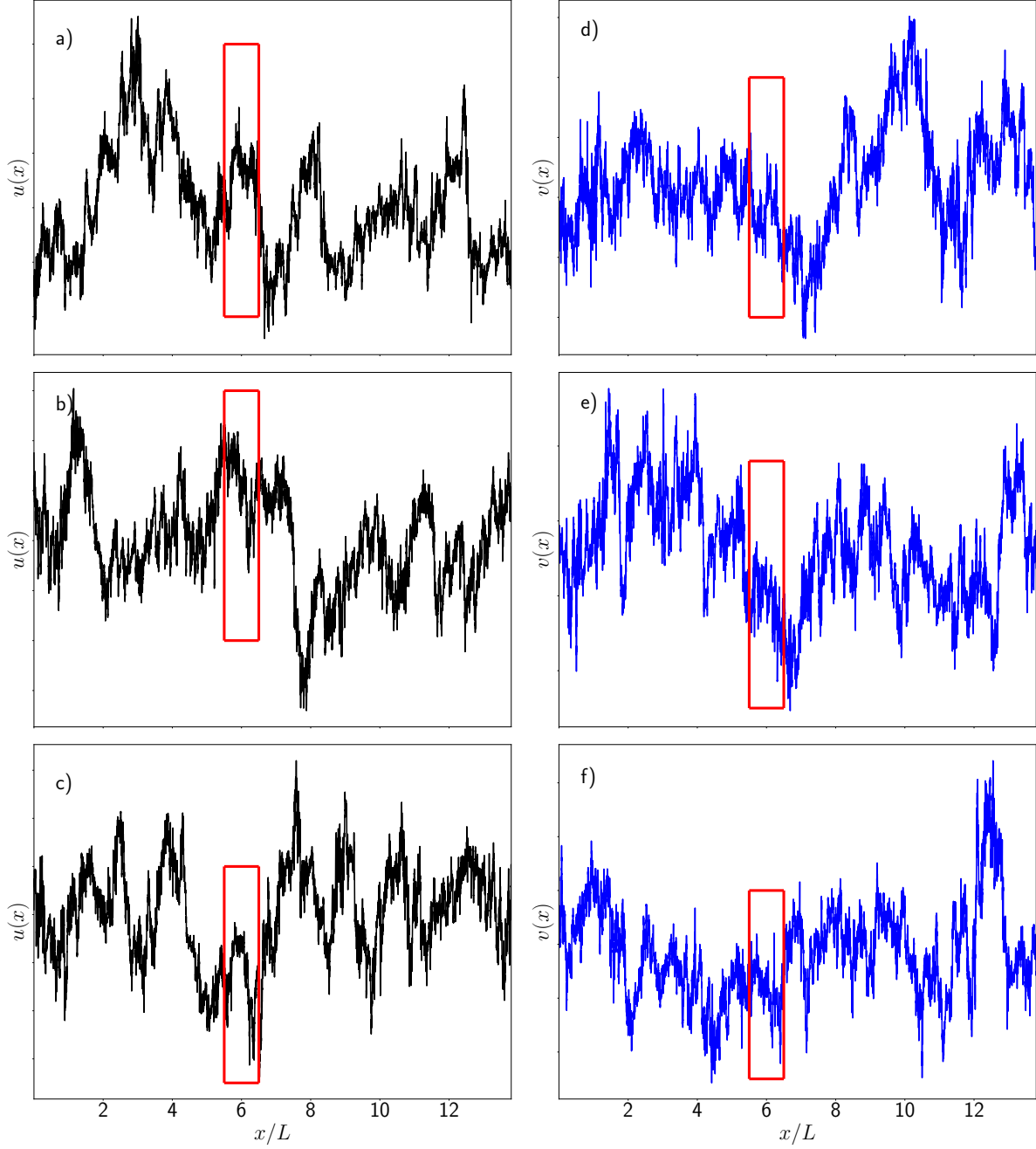


Figure 5. Illustration of three realizations of the process $u(x)$ generated with our GAN approach a), b) and c) and three realizations of Modane velocity measures $v(x)$ d), e) and f), in function of the spatial variable x/L . The red boxes correspond to the length of a Modane integral scale L .

fields, the large scales in the integral domain are Gaussian and the more energetic ones. Then, when the scale decreases the energy decreases and the PDFs become assymmetric and heavy-tailed. Furthermore, the energy distribution, skewness and flatness of $u(x)$ closely follow, within the errorbars, the ones of Modane. However, we can observe oscillations in the flatness and the skewness of the generated field that are not present

in the Modane one. Actually, these measures are very sensitive to small changes in the PDFs and point out minor behaviors that are not perceptible when looking directly at the structure functions.

These results are supported by figure 7 which illustrates the PDF of several velocity increments of Modane a) and c) and the generated field b) and d) for scales in the integral, inertial and dissipative domains. While the histograms of a) and b) are done taking into account respectively the whole Modane and generated dataset (256 realizations of size N), the histograms of c) and d) are done with only one segment of size N as the ones used during training. We compare first the full PDFs of Modane a) and the generated field b). Both processes present Gaussian PDFs at scales in the integral domain which become the more and more assymmetric and heavy-tailed when the scale decreases through the inertial and dissipative domains. The deformation of the PDF of $u(x)$ across scales is very close to the one of Modane. However in the dissipative domain the Modane PDFs present stronger extreme events than the ones of the generated field. Indeed, our generative model is trained with single realizations of size N of Modane, which exhibit few extreme events at small scales as shown by figure 7 c). Looking at single realizations, the PDFs of the generated field d) are almost indistinguishable from the Modane ones c) and the few extreme events are well captured. This explains the good similarity between PDFs in a) and b). Nevertheless, still rarer extreme events in Modane are not learned by our model and lead to the slightly heavier tails of a) compared to b).

Figure 8 shows the scaling exponent ζ_p in function of p for Modane in blue and the generated field in black, as well as the behavior predicted by the Kolmogorov 1941 theory in red. The scaling exponents of $v(x)$ and $u(x)$ are obtained by fitting the slope of $\log(S_p(l))$ vs $\log(l)$ in the inertial region far away from η and L . In this study we used $17l_s < l < 274l_s$ to define the fitting region. Both Modane and $u(x)$ present a non-linear scaling function matching within the errorbars. Finally, $u(x)$ has $\zeta_3 = 1$ and so it respects the 4/5 law of Kolmogorov.

Two alternative models from the state of the art were also tested. First, a classical GAN model [15] and second a Wasserstein GAN (WGAN) model [42], both with the generator presented in section 3.1 and the discriminator following the architecture of one of the networks of the *scale-invariance* discriminator of section 3.2 but applied directly on signals of size N . Results presented in Appendix A show that these models do not allow to generate stochastic fields with turbulent velocity statistics. This illustrates the contribution of our multiscale multicriteria physics based approach.

5. Conclusions

We present a neural network generator model embedded in a multicriteria GAN learning strategy for the synthesis of a 1-dimensional stochastic field with turbulent statistics. The presented approach is guided by the multiscale physics of turbulence in two ways. First, the generator architecture is fully convolutional mimicking the

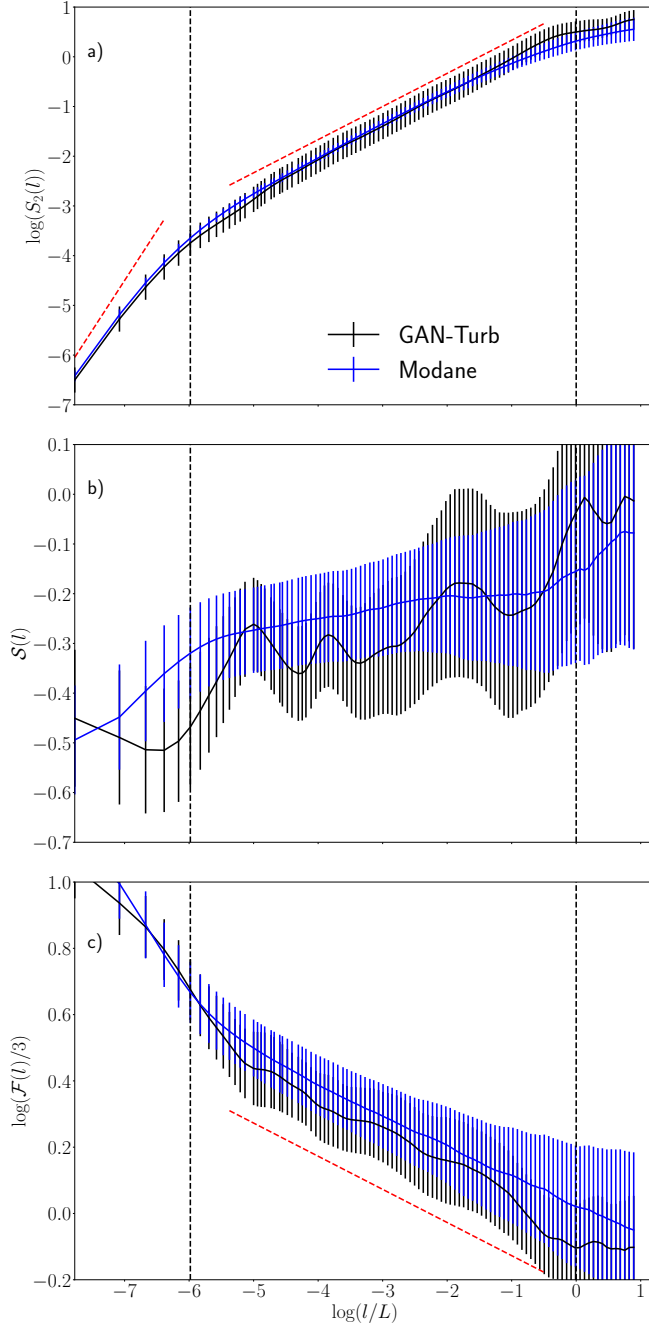


Figure 6. a) Logarithm of the second order structure function $\log(S_2(l))$, b) skewness $S(l)$ and c) logarithm of the flatness $\log(\mathcal{F}(l)/3)$ in function of the logarithm of the scale of analysis $\log(l/L)$ for our GAN generated field (black) and Modane (blue). Curves represent the mean value and errorbars the standard deviation calculated on 256 realizations. Red dashed lines in a) have a slope 2 in the dissipative domain and $2/3$ in the inertial one describing respectively the behaviors of the Batchelor model [41] and the $2/3$ Kolmogorov law. Red dashed line in c) has a slope -0.1 previously described for the $\log(\mathcal{F}(l)/3)$ in the inertial domain [11]. The vertical black dashed lines correspond to the Kolmogorov η and integral L scales of Modane.

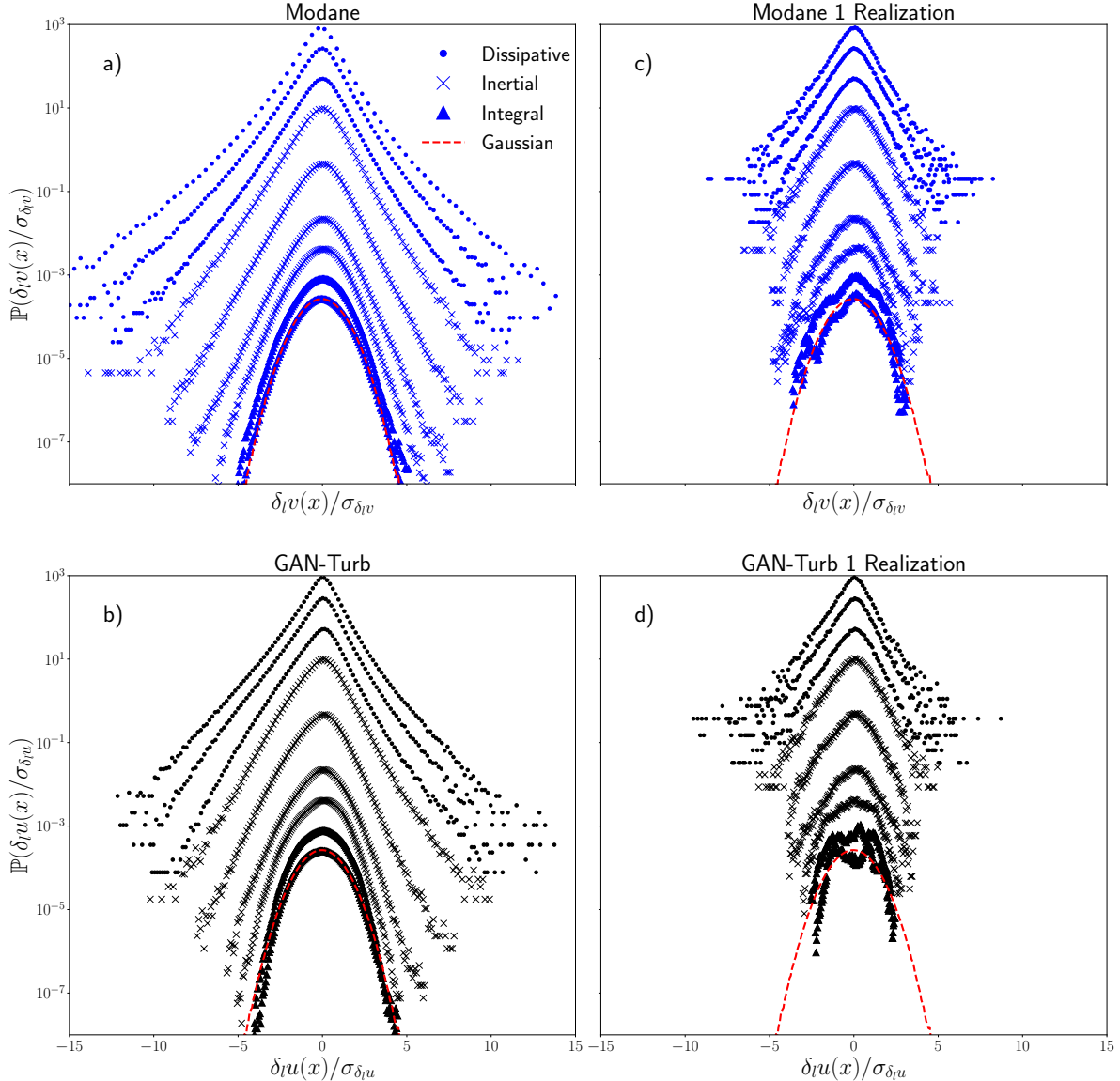


Figure 7. Logarithm of the probability density function of the centered and standardized increments of the Modane turbulent velocity signal, a) and c), and the GAN fields, b) and d), in function of the values of the standardized increments. PDFs from a) and b) are obtained from 256 realizations of size N and PDFs from c) and d) from only 1 realization of size N . The illustrated increments are those with $l = \{2, 4, 8, 16, 64, 256, 1024, 4096, 10000\} l_s$. The integral scale of the flow is $L = 2350 l_s$. The red dashed line corresponds to the logarithm of the probability density function of a centered and standardized Gaussian distribution.

multiresolution analysis usually done to characterize turbulent velocity across scales. Second, the training schema is based on four discriminators each one focusing on a given statistical property of turbulence: 1) variance, 2) skewness and 3) flatness of the velocity increments across scales, which are respectively linked to the energy distribution, energy cascade and intermittency phenomenon, and 4) the full PDF of the velocity field at different scales of resolution.

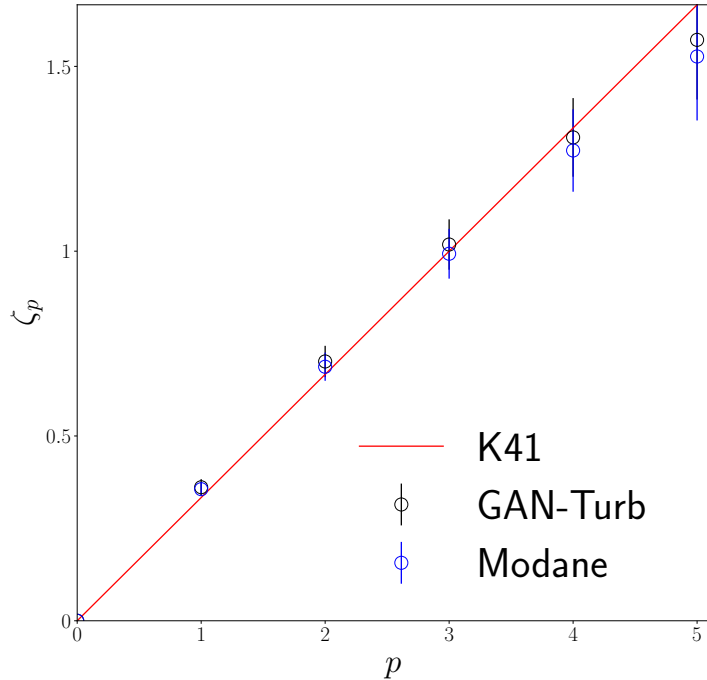


Figure 8. Scaling function ζ_p of the Kolmogorov 1941 model in red, Modane velocity turbulent dataset in blue and the GAN velocity field in black in function of p .

Consequently, this model is able to generate an intermittent and scale-invariant stochastic field $u(x)$. This field exhibits three domains of scales with different statistical behavior as well as the energy distribution and the energy cascade of turbulence as illustrated by $S_2(l)$ and $\mathcal{S}(l)$ respectively. Furthermore this field presents a deformation of the PDF of its increments which goes from Gaussian at large scale to heavy-tailed and asymmetric at small scales such as the PDF of the turbulent velocity increments. This is illustrated by $\mathcal{S}(l)$, $\mathcal{F}(l)$ and ζ_p . Moreover, looking at the PDFs of the increments of $u(x)$ computed on 256 realizations of size N , we observe that the model is able to recover extreme events that do not appear in single realizations of the same size, as the ones used during training. Contrary to most of previous work on neural network modelling of turbulence [29, 30, 31, 43], we not only focus on second order statistics of the velocity field, but also on higher-order statistics, more precisely on the skewness and flatness of the velocity increments that are theoretically linked with the energy cascade and intermittency.

We compare the stochastic field generated with our physics based multiscale approach to two stochastic fields generated by state of the art methods: a classical GAN and a Wasserstein GAN. Our approach clearly outperforms the state of the art ones.

Stochastic generative models such as the one presented in this work allow the generation of large amounts of data with specific statistics which are useful for validating methodologies of analysis [44] or feeding machine learning algorithms when real data are scarce [45, 46]. Furthermore, generative models provide new insights into the

studied process itself by characterizing how the model operates to produce the stochastic field [43]. In addition, many processes from different fields such as geophysics [47, 48], finance [49, 9, 50], biomedicine [51, 52], biology [53] or telecommunications [54, 55] present complex dynamics requiring higher-order statistics for a correct modelling, and so our model can find applications in a large range of domains.

Finally, the main future perspective is to generalize the proposed approach to synthesize 2d stochastic fields with the statistics of homogeneous and isotropic turbulent velocity. Furthermore, we consider to generalize the current physics based multiscale generative model by conditioning it on the Reynolds number of the flow. The multiscale and multicriteria physics based GAN used in this work is available at <https://github.com/manuelcgallucci/DCGAN-turb>.

Acknowledgments

This work was supported by the French National Research Agency (ANR-21-CE46-0011-01), within the program "Appel à projets générique 2021".

Appendix A. Results with GAN and Wasserstein GAN models

This section illustrates the performances of two state of the art neural network models, a classical GAN and a Wasserstein GAN, when dealing with the generation of a 1-dimensional stochastic field with turbulent statistics. Both models use the generator presented in section 3.1 and a discriminator with the architecture of one of the networks of the *scale-invariance* discriminator of section 3.2 but applied directly on the generated and Modane signals.

Figure A1 shows three realizations of the GAN and WGAN models in green and magenta respectively and three realizations of the Modane turbulent velocity field in blue for comparison. While the GAN field is visually very close to the Modane one with large and small scale structures of similar sizes, this is not the case for the WGAN which presents very energetic small scales and few large scale structures.

This visual conclusion is supported by figure A2 a) which shows $\log(S_2(l))$ in function of the logarithm of the scale of analysis for the GAN (green), WGAN (magenta) and Modane (blue) fields. Both the GAN and WGAN fields present small scales that are too energetic compared to Modane and slopes in the inertial domain smaller than the expected 2/3 value. Figures A2 b) and c) present respectively the skewness and flatness of the GAN, WGAN and Modane fields. For both models the skewness and flatness strongly oscillate and are far from the Modane ones in several domains of scales.

Figure A3 presents the logarithm of the PDF of the standardized and centered increments of the GAN, WGAN and Modane velocity fields. Again, the stochastic field generated with the WGAN model presents PDFs with shapes very different from Modane while the shapes of the PDFs of the field generated with the classical GAN are visually very similar. However even for the GAN field, figure A2 quantifies the strong

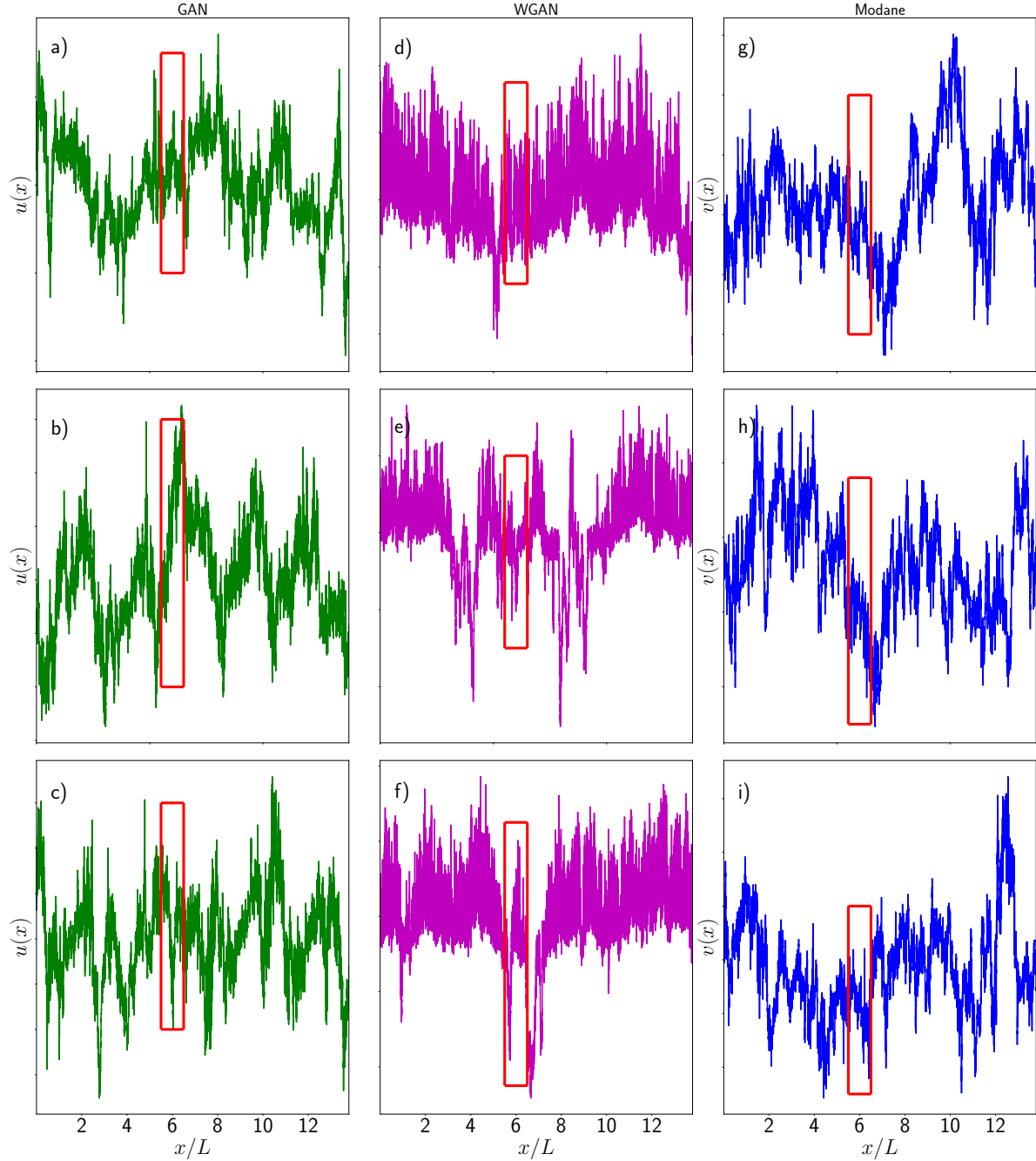


Figure A1. Illustration of three realizations of the process $u(x)$ generated with a classical GAN a), b) and c), a Wasserstein GAN d), e) and f) and three realizations of Modane velocity measures $v(x)$ g), h) and i), in function of the spatial variable x/L . The red boxes correspond to the length of a Modane integral scale L .

differences between the shapes of the PDFs of Modane and the classical GAN field.

Figure A4 shows the behavior of the scaling function ζ_p in function of p for the Modane (blue), GAN (green) and WGAN (magenta) field, and provides a clear illustration of the absence of physical sens of the generated fields. As said in section 2, ζ_3 must be equal to 1 for turbulence, and this is not the case for either the classical

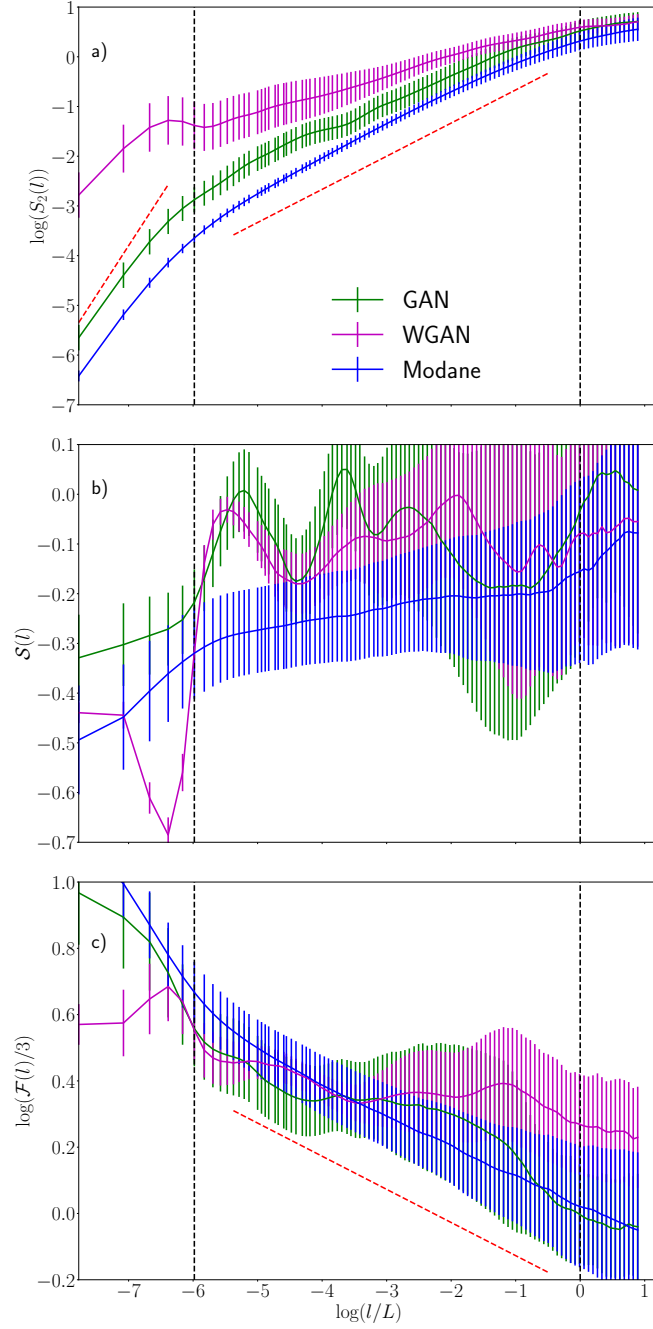


Figure A2. a) Logarithm of the second order structure function $\log(S_2(l))$, b) skewness $S(l)$ and c) logarithm of the flatness $\log(\mathcal{F}(l)/3)$ in function of the logarithm of the scale of analysis $\log(l/L)$ for a stochastic field generated with a classical GAN (green) a Wasserstein GAN (magenta) and the velocity field of Modane (blue). Curves represent the mean value and errorbars the standard deviation calculated on 256 realizations. Red dashed lines in a) have a slope 2 in the dissipative domain and $2/3$ in the inertial one describing respectively the behaviors of the Batchelor model [41] and the $2/3$ Kolmogorov law. Red dashed line in c) has a slope -0.1 previously described for the $\log(\mathcal{F}(l)/3)$ in the inertial domain [11]. The vertical black dashed lines correspond to the Kolmogorov η and integral L scales of Modane.

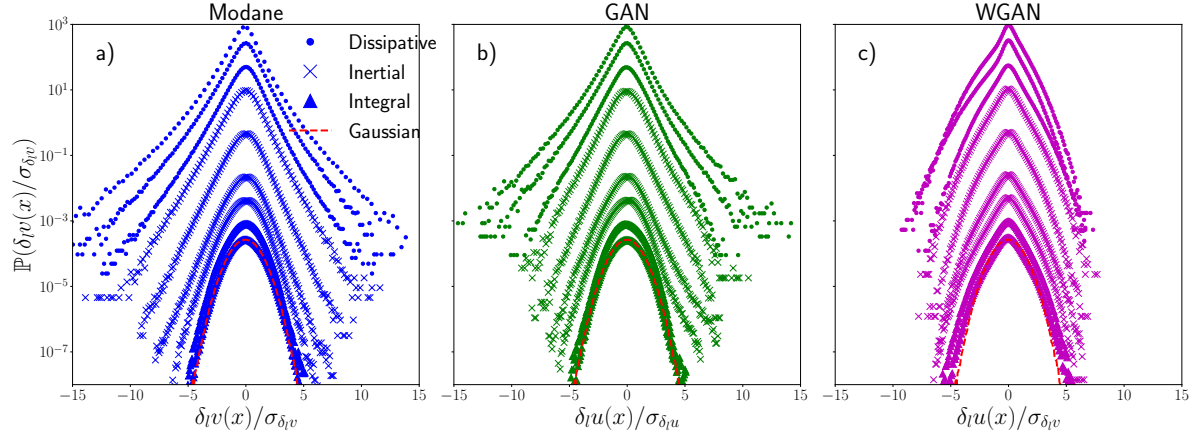


Figure A3. Logarithm of the probability density function of the centered and standardized increments of the Modane turbulent velocity signal a) a classical GAN field b) and a Wasserstein GAN field c), in function of the values of the standardized increments. The PDFs are obtained from 256 realizations of size N of the fields. The illustrated increments are those with $l = \{2, 4, 8, 16, 64, 256, 1024, 4096, 10000\} l_s$. The integral scale of the flow is $L = 2350 l_s$. The red dashed line corresponds to the logarithm of the probability density function of a centered and standardized Gaussian distribution.

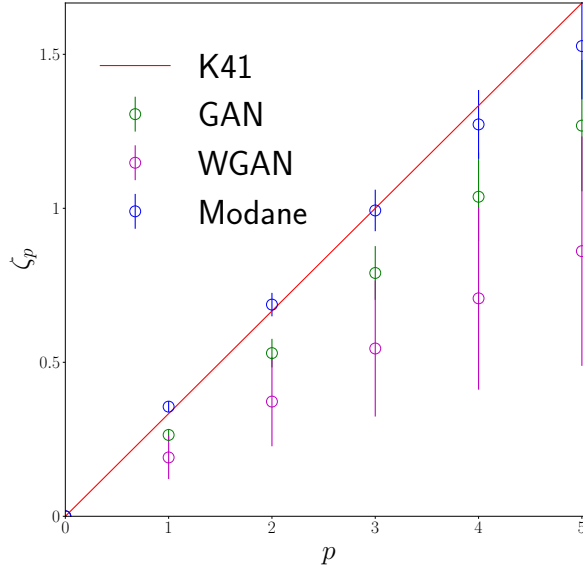


Figure A4. Scaling function ζ_p of the Kolmogorov 1941 model in red, Modane velocity turbulent dataset in blue, classical GAN velocity field in green and Wasserstein GAN field in magenta, in function of p .

GAN or the WGAN.

So, we conclude that our GAN-Turb model outperforms state of the art ones, and generates a physical stochastic field with turbulent statistics.

- [1] A. N. Kolmogorov. The local structure of turbulence in incompressible viscous fluid for very large Reynolds numbers. *Proceedings: Mathematical and Physical Sciences*, 434(1890):9–13, 1991.
- [2] A. N. Kolmogorov. A refinement of previous hypotheses concerning the local structure of turbulence in a viscous incompressible fluid at high Reynolds number. *Journal of Fluid Mechanics*, 13:82–85, 1962.
- [3] A. M. Obukhov. Some specific features of atmospheric turbulence. *Journal of Fluid Mechanics*, 13:77–81, 1962.
- [4] U. Frisch. *Turbulence: the legacy of A.N. Kolmogorov*. Cambridge University Press, 1995.
- [5] P. Flandrin. On the spectrum of fractional Brownian motions. *IEEE Transactions on Information Theory*, 35(1):197–199, 1989.
- [6] P. Flandrin. Wavelet analysis and synthesis of fractional Brownian motion. *IEEE Transactions on Information Theory*, 38(2):910–917, 1992.
- [7] R. Benzi, L. Biferale, A. Crisanti, G. Paladin, M. Vergassola, and A. Vulpiani. A random process for the construction of multi-affine fields. *Physica D*, 65(4):352–358, 1993.
- [8] A. Arneodo, E. Bacry, and J. F. Muzy. Random cascades on wavelet dyadic trees. *Journal of Mathematical Physics*, 39(8):4142–4164, 1998.
- [9] E. Bacry, J. Delour, and J. F. Muzy. Multifractal random walk. *Physical Review E*, 64:026103, 2001.
- [10] R. Robert and V. Vargas. Hydrodynamic turbulence and inter-mittent random fields. *Communications in Mathematical Physics*, 284:649, 2008.
- [11] L. Chevillard, B. Castaing, A. Arneodo, E. Lévéque, J.F. Pinton, and S.G. Roux. A phenomenological theory of eulerian and lagrangian velocity fluctuations in turbulent flows. *Comptes Rendus Physique*, 13(9):899 – 928, 2012.
- [12] Y. Du and G. Lin. Turbulence generation from a stochastic wavelet model. *Proceedings of the Royal Society A*, 474:20180093, 2018.
- [13] L. Chevillard, C. Garban, R. Rhodes, and V. Vargas. On a skewed and multifractal unidimensional random field, as a probabilistic representation of Kolmogorov’s views on turbulence. *Annales Henri Poincaré*, 20:3693–3741, 2019.
- [14] A. V. Alexandrov, L. W. Dorodnicyn, A. P. Duben, and D. R. Kolyukhin. Generation of the stochastic anisotropic velocity field for turbulent flow simulation. In *AIP Conference Proceedings*, volume 2312, page 050001, 2020.
- [15] I. Goodfellow, J. Pouget-Abadie, M. Mirza, B. Xu, D. Warde-Farley, S. Ozair, A. Courville, and Y. Bengio. Generative Adversarial Nets. In *Advances in Neural Information Processing Systems*, volume 27, 2014.
- [16] T. Beroud, P. Abry, Y. Malevergne, M. Senneret, G. Perrin, and J. Macq. Wasserstein GAN synthesis for time series with complex temporal dynamics: frugal architectures and arbitrary sample-size generation. In *IEEE International Conference on Acoustics, Speech and Signal Processing (ICASSP)*, pages 1–5, Rhodes Island, Greece, 2023.
- [17] Y. Song and S. Ermon. Generative modeling by estimating gradients of the data distribution. In *Advances in Neural Information Processing Systems*, volume 32, 2019.
- [18] T. Yan, H. Zhang, T. Zhou, Y. Zhan, and Y. Xia. ScoreGrad: multivariate probabilistic time series forecasting with continuous energy-based generative models, 2021.
- [19] P. Dhariwal and A. Nichol. Diffusion models beat GANs on image synthesis. In *Advances in Neural Information Processing Systems*, volume 34, pages 8780–8794, 2021.
- [20] Z. Zhang, R. Zhang, Z. Li, Y. Bengio, and L. Paull. Perceptual generative autoencoders. In *Proceedings of the 37th International Conference on Machine Learning*,, volume 119, pages 11298–11306, 2020.
- [21] F. Ye and A. G. Bors. Deep mixture generative autoencoders. *IEEE Transactions on Neural Networks and Learning Systems*, 33(10):5789–5803, 2022.
- [22] S. L. Brunton, B. R. Noack, and P. Koumoutsakos. Machine learning for fluid mechanics. *Annual Review of Fluid Mechanics*, 52:477–508, 2020.

- [23] A. Beck and M. Kurz. A perspective on machine learning methods in turbulence modeling. *Surveys for Applied Mathematics and Mechanics*, 44:e202100002, 2021.
- [24] Z. Deng, C. He, Y. Liu, and K. C. Kim. Super-resolution reconstruction of turbulent velocity fields using a generative adversarial network-based artificial intelligence framework. *Physics of Fluids*, 31:125111, 2019.
- [25] B. Liu, J. Tang, H. Huang, and X. Y. Lu. Deep learning methods for super-resolution reconstruction of turbulent flows. *Physics of fluids*, 32(2):025105, 2020.
- [26] J. Kim and C. Lee. Deep unsupervised learning of turbulence for inflow generation at various Reynolds numbers. *Journal of Computational Physics*, 406:109216, 2020.
- [27] H. Kim, J. Kim, S. Won, and C. Lee. Unsupervised deep learning for super-resolution reconstruction of turbulence. *Journal of Fluid Mechanics*, 910:A29, 2021.
- [28] B. Kim, V. C. Azevedo, N. Thuerey, T. Kim, M. Gross, and B. Solenthaler. Deep fluids: A generative network for parameterized fluid simulations. *Computer Graphics Forum*, 38(2):59–70, 2019.
- [29] J.-L. Wu, K. Kashinath, A. Albert, D. Chirila, Prabhat, and H. Xiao. Enforcing statistical constraints in generative adversarial networks for modeling chaotic dynamical systems. *Journal of Computational Physics*, 406:109209, 2020.
- [30] M. Z. Yousif, L. Yu, and H.-C. Lim. High-fidelity reconstruction of turbulent flow from spatially limited data using enhanced super-resolution generative adversarial network. *Physics of Fluids*, 33:125119, 2021.
- [31] M. Z. Yousif, L. Yu, and H.-C. Lim. Super-resolution reconstruction of turbulent flow fields at various Reynolds numbers based on generative adversarial networks. *Physics of Fluids*, 34:015130, 2022.
- [32] M. Yousif, L. Yu, and H. Lim. Physics-guided deep learning for generating turbulent inflow conditions. *Journal of Fluid Mechanics*, 936:A21, 2022.
- [33] L. F. Richardson. Some measurements of atmospheric turbulence. *Philosophical Transactions of the Royal Society of London. Series A: Containing papers of a mathematical or physical character*, 221:1–28, 1921.
- [34] T. von Kármán and L. Howarth. On the statistical theory of isotropic turbulence. *Proceedings of the Royal Society of London A*, 164:192–215, 1938.
- [35] Y. Gagne, E. J. Hopfinger, and U. Frisch. *New trends in nonlinear dynamics and pattern-forming phenomena*, volume 237 of *NATO ASI Series*, chapter A new universal scaling for fully developed turbulence: the distribution of velocity increments, pages 315–319. Springer, New York, 1990.
- [36] H. Kahalerras, Y. Malecot, Y. Gagne, and B. Castaing. Intermittency and Reynolds number. *Physics of Fluids*, 10:910–921, 1998.
- [37] C. Granero-Belinchon, S. G. Roux, and N. B. Garnier. Scaling of information in turbulence. *EuroPhysics Letters*, 115(5):58003, 2016.
- [38] A. Arneodo, S. Manneville, J. F. Muzy, and S. G. Roux. Revealing a lognormal cascading process in turbulent velocity statistics with wavelet analysis. *Philosophical transactions: mathematical, physical and engineering sciences*, 357(1760):2415–2438, 1999.
- [39] O. Ronneberger, P. Fischer, and T. Brox. U-Net: convolutional networks for biomedical image segmentation. In *Medical Image Computing and Computer-Assisted Intervention – MICCAI 2015*, pages 234–241, 2015.
- [40] I. Goodfellow, Y. Bengio, and A. Courville. *Deep Learning*. MIT Press, 2016. <http://www.deeplearningbook.org>.
- [41] G. K. Batchelor. Pressure fluctuations in isotropic turbulence. *Mathematical Proceedings of the Cambridge Philosophical Society*, 47:359–374, 1951.
- [42] M. Arjovsky, S. Chintala, and L. Bottou. Wasserstein Generative Adversarial Networks. In *Proceedings of the 34th International Conference on Machine Learning*, volume 70, pages 214–223, Sydney, Australia, August 2017.
- [43] A. Subel, Y. Guan, A. Chattopadhyay, and P. Hassanzadeh. Explaining the physics of transfer

learning in data-driven turbulence modeling. *PNAS Nexus*, 2(3):pgad015, 2023.

[44] C. Granero-Belinchon, S. G. Roux, P. Abry, and N. B. Garnier. Probing high-order dependencies with information theory. *IEEE Transactions on Signal Processing*, 67(14):3796–3805, 2019.

[45] R. J. Chen, M. Y. Lu, T. Y. Chen, D. F. K. Williamson, and F. Mahmood. Synthetic data in machine learning for medicine and healthcare. *Nature Biomedical Engineering*, 5:493–497, 2021.

[46] C. Gao, B. D. Killeen, Y. Hu, R. B. Grupp, R. H. Taylor, M. Armand, and M. Unberath. Synthetic data accelerates the development of generalizable learning-based algorithms for X-ray image analysis. *Nature Machine Intelligence*, 5:294–308, 2023.

[47] B. Khouider, A. J. Majda, and M. A. Katsoulakis. Coarse-grained stochastic models for tropical convection and climate. *Proceedings of the National Academy of Sciences*, 100(21):11941–11946, 2003.

[48] B. Chapron, P. Derian, E. Memin, and V. Resseguier. Large-scale flows under location uncertainty: a consistent stochastic framework. *Quarterly Journal of the Royal Meteorological Society*, 144(710):251–260, 2018.

[49] J. F. Muzy, J. Delour, and E. Bacry. Modelling fluctuations of financial time series: from cascade process to stochastic volatility model. *The European Physical Journal B*, 17:537–548, 2000.

[50] J. Han, X.-P. Zhang, and F. Wang. Gaussian process regression stochastic volatility model for financial time series. *IEEE Journal of Selected Topics in Signal Processing*, 10(6):1015–1028, 2016.

[51] A. Ochab-Marcinek and E. Gudowska-Nowak. Population growth and control in stochastic models of cancer development. *Physica A*, 343:557–572, 2004.

[52] M. Baar, L. Coquille, H. Mayer, M. Holzel, M. Rogava, T. Tuting, and A. Bovier. A stochastic model for immunotherapy of cancer. *Scientific Reports*, 6:24169, 2016.

[53] F. Schmitt and L. Seuront. Multifractal random walk in copepod behavior. *Physica A*, 301:375–396, 2001.

[54] C. Gloaguen, F. Fleischer, H. Schmidt, and V. Schmidt. Fitting of stochastic telecommunication network models via distance measures and Monte–Carlo tests. *Telecommunication systems*, 31:353–377, 2006.

[55] A. Eisenblatter and J. Schweiger. Multistage stochastic programming in strategic telecommunication network planning. *Computational Management Science*, 9:303–321, 2012.